APL Materials

RESEARCH ARTICLE | NOVEMBER 20 2019

Epitaxial κ-$(Al_xGa_{1-x})_2O_3$ thin films and heterostructures grown by tin-assisted VCCS-PLD

P. Storm ; M. Kneiß ; A. Hassa ; T. Schultz ; D. Splith ; H. von Wenckstern ; N. Koch ; M. Lorenz ; M. Grundmann

APL Mater. 7, 111110 (2019)
https://doi.org/10.1063/1.5124231

Epitaxial κ-$(Al_xGa_{1-x})_2O_3$ thin films and heterostructures grown by tin-assisted VCCS-PLD

Cite as: APL Mater. 7, 111110 (2019); doi: 10.1063/1.5124231
Submitted: 12 August 2019 • Accepted: 30 October 2019 •
Published Online: 20 November 2019

View Online Export Citation CrossMark

P. Storm,[1,a] M. Kneiß,[1] A. Hassa,[1] T. Schultz,[2,3] D. Splith,[1] H. von Wenckstern,[1] N. Koch,[2,3] M. Lorenz,[1] and M. Grundmann[1]

AFFILIATIONS

[1] Felix Bloch Institute for Solid State Physics, Universität Leipzig, Linnéstraße 5, 04103 Leipzig, Germany
[2] Department of Physics, Humboldt Universität zu Berlin, Newtonstraße 15, 12489 Berlin, Germany
[3] Helmholtz-Zentrum Berlin für Materialien und Energie GmbH, Hahn-Meitner-Platz 1, 14109 Berlin, Germany

[a] **Electronic mail:** philipp.storm@studserv.uni-leipzig.de

ABSTRACT

The structural, surface, and optical properties of phase-pure κ-$(Al_xGa_{1-x})_2O_3$ thin films on c-sapphire and STO(111):Nb substrates as well as on MgO(111) and κ-Ga_2O_3 templates are reported as a function of alloy composition for $x < 0.4$. The thin films were grown by tin-assisted pulsed laser deposition (PLD). For the variation of the Al-content, we utilized radially segmented PLD targets that enable the deposition of a thin film material library by discrete composition screening. Growth on κ-Ga_2O_3 (001) thin film templates enhanced the phase pure growth window remarkably up to $x = 0.65$. The crystallization of the κ-phase was verified by X-ray diffraction 2θ-ω-scans for all samples. Both in- and out-of-plane lattice constants in dependence on the Al-content follow a linear relationship according to Vegard's law over the complete composition range. Atomic force microscope measurements confirm smooth surfaces ($R_q \approx 1.4$ nm) for all investigated Al-contents. Furthermore, bandgap tuning from 4.9 eV to 5.8 eV is demonstrated and a linear increase in the bandgap with increasing Al-content was observed.

I. INTRODUCTION

Recently, the transparent semiconductor Ga_2O_3 gained considerable attention due to its interesting physical properties such as wide bandgap[1] and high electrical breakdown field[2] enabling a variety of potential applications such as high power transistors, solar blind photodetectors, and gas sensors.[3–5] The most intensively investigated polymorph of Ga_2O_3 is the monoclinic β phase because of its thermodynamic stability at standard environmental conditions. However, more and more attention is presently shifting toward other polymorphs of Ga_2O_3. In particular, the orthorhombic κ-phase,[6] also referred to as ε-phase, gained a significant degree of interest due to its high predicted spontaneous polarization[7] of 23 $\mu C/cm^2$. This presumably leads to the formation of a 2 dimensional electron gas at κ-Ga_2O_3/GaN,[8] κ-Ga_2O_3/$CaCO_3$,[9] or κ-Ga_2O_3/κ-$(Al,Ga)_2O_3$ heterointerfaces, acting as a functional layer in various device applications such as high power devices operating at high frequencies.[9] However, the atomic displacements in the unit cell of κ-Ga_2O_3 indicate a remarkably lower spontaneous polarization of only 0.2 $\mu C/cm^2$ as revealed by Cora *et al.*[6] Therefore, more work is required to determine the true capabilities of κ-Ga_2O_3 for such applications. The heteroepitaxial growth of κ-Ga_2O_3 has already been achieved by metal organic chemical vapor deposition (MOCVD),[10–15] halide vapor phase epitaxy (HVPE),[16] mist chemical vapor deposition (MCVD),[17,18] laser molecular beam epitaxy,[19] molecular beam epitaxy (MBE),[20] as well as pulsed laser deposition (PLD).[21,22] To stabilize the κ-phase of Ga_2O_3 in MBE and PLD, the presence of tin is crucial as it acts as a catalyst and is not significantly incorporated into the thin film.[20,21] Recently, the first paper reporting on conductive n-type κ-Ga_2O_3 was published, utilizing Sn and Si

as donors elements,[23] and with this opening perspectives in practical device applications.

Alloying of Ga_2O_3 with indium and aluminum in the β-phase has already been achieved and is well investigated regarding various material properties and heterostructures.[24–33] However, for the κ-phase, investigations of the alloy system are at their beginning. Only a few reports concerning bandgap engineering, growth, and optical properties of κ-$(In,Ga)_2O_3$ grown by PLD[34] and MCVD[35] or κ-$(Al,Ga)_2O_3$ grown by MCVD[36] are available. Reports related to the growth of κ-Ga_2O_3 heterostructures are so far not published.

In this work, the tin-assisted heteroepitaxial growth of κ-$(Al,Ga)_2O_3$ by PLD on c-sapphire and STO(111):Nb substrates as well as κ-Ga_2O_3(001) and MgO(111) templates is presented. A new PLD technique, referred to as VCCS-PLD (vertical continuous composition spread-PLD) was employed.[37] By variation of the radial position of the PLD laser spot on an elliptically segmented target, the composition of the particle flux toward the substrate may be varied, resulting in thin films with distinct composition or continuous vertical composition spread. In this report, the VCCS-technique was utilized for the growth of thin films with discrete and vertical homogeneous compositions. This allows for the growth of a set of differently composed samples using one and the same PLD-target. The resulting thin films were investigated regarding morphological and structural properties, optical bandgaps, and epitaxial growth in dependence on growth parameters and aluminum contents.

II. EXPERIMENTAL METHODS

The targets utilized for the aluminum variation in this report consist of $(Al_{0.4}Ga_{0.6})_2O_3$ + 1.5 at. % SnO_2 or $(Al_{0.2}Ga_{0.8})_2O_3$ + 1.5 at. % SnO_2 in the outer segment and Ga_2O_3 + 1.5 at. % SnO_2 in the inner segment of the elliptically segmented target [Fig. 1(c)]. The optimization of the growth parameters was conducted employing a target with $(Al_{0.1}Ga_{0.9})_2O_3$ + 1 at. % SnO_2 in the outer and $(Al_{0.1}Ga_{0.9})_2O_3$ in the inner segment of the target. Ga_2O_3 (99.999% purity), Al_2O_3 (99.997% purity), and SnO_2 (99.9% purity) powders from Alfa Aesar were utilized. To achieve the segmentation of the target, a stainless steel form was used resulting in a target with ≈28 mm outer diameter, comprising an inner segment with a height of ≈17 mm and a width of ≈7 mm. To produce the targets, Al_2O_3, Ga_2O_3, and SnO_2 powders were presintered in air at 1150 °C for

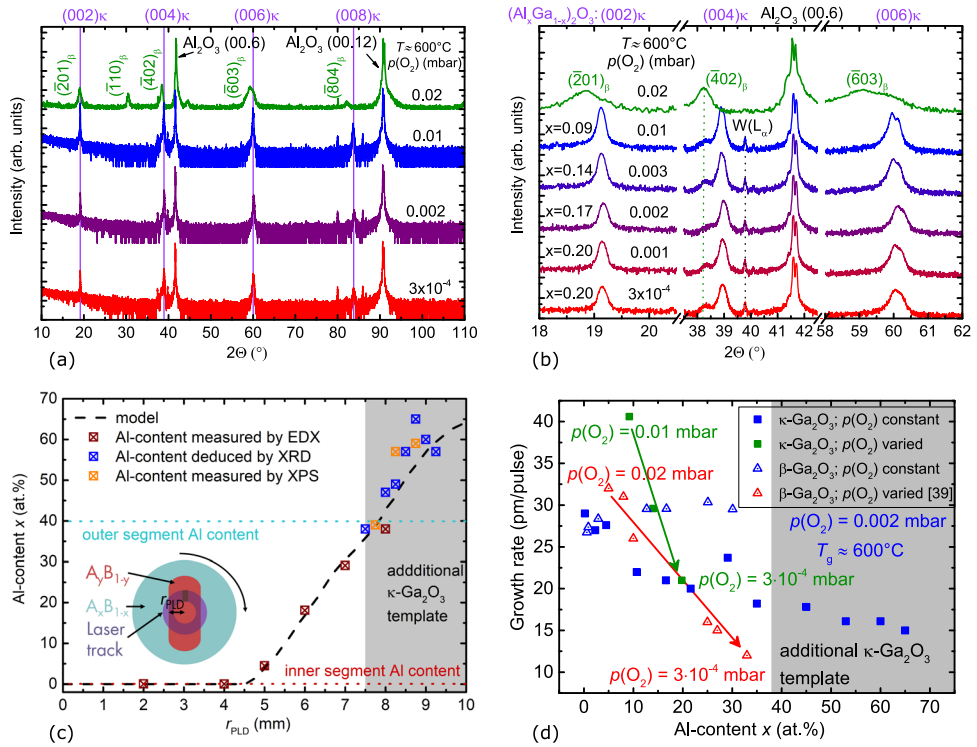

FIG. 1. (a) Wide-angle XRD 2θ-ω scans of samples grown with oxygen pressure variation on c-sapphire. The growth temperature was kept constant at $T \approx 600$ °C. The green diffractogram represents the β-phase which is stabilized for $p(O_2) = 0.02$ mbar. (b) (002), (004), and (006) κ-$(Al_xGa_{1-x})_2O_3$ peaks in a magnified view with Al-contents as labeled. W(L_α) denotes reflections due to tungsten L_α radiation. (c) Aluminum content in dependence on the radial position r_{PLD} of the PLD laser spot on the target. The compositions were determined by EDX, XPS, and XRD peak positions. (d) Growth rates for various κ-$(Al_xGa_{1-x})_2O_3$ (green and blue squares) and β-$(Al_xGa_{1-x})_2O_3$ (blue and red triangles) thin films as determined by ellipsometry and XRR in comparison. The data for the pressure varied β-phase layers were extracted from[40] where the same PLD-setup was used with the pressure range as indicated. The target utilized for these thin films consists of 86.8 at. % Ga_2O_3 + 8.8 at. % Al_2O_3 + 4.4 at. % SiO_2. The β-Ga_2O_3 thin films at constant pressure were deposited employing an elliptically segmented target with 79.5 at. % Ga_2O_3 + 20 at. % Al_2O_3 + 0.5 at. % SnO_2 in the outer and 99.5 at. % Ga_2O_3 + 0.5 at. % SnO_2 and variation of the PLD laser spot radius r_{PLD} (VCCS-PLD).

10 h, ball-milled, pressed, and subsequently sintered at 1350 °C for 72 h. For the growth of the κ-Ga_2O_3 templates, a homogeneous target consisting of Ga_2O_3 + 1 at. % Sn was employed. For the growth of the MgO templates, a homogeneous MgO target was used, which was produced from MgO-powders (Alfa Aesar, 99.998% purity) and sintered at 1650 °C for 6 h. The PLD system employed consists of a Coherent LPXpro 305 248 nm KrF excimer laser. The laser operates at a pulse energy of ≈650 mJ, resulting in an energy density on the target surface of ≈2.6 J cm^{-2} with a pulse frequency of 10 Hz. The growth pressure was varied between 3×10^{-4} mbar O_2 and 0.02 mbar O_2. X-ray diffraction (XRD) measurements were performed with a PANalytical X'Pert PRO Materials Research Diffractometer (MRD) with Cu K_α radiation equipped with a PIXcel^{3D} detector with 255 × 255 pixels. ϕ-scans, 2θ-ω-scans, as well as reciprocal space maps (RSM) and X-ray reflectivity (XRR)-scans were measured. The aluminum content was determined by energy-dispersive X-ray spectroscopy (EDX) with a Nova NanoLab 200 by FEI company. Due to the strong depth sensitivity of EDX and the associated uncertainties for samples produced on Ga_2O_3 templates, X-ray photoelectron spectroscopy (XPS) measurements were conducted as they are more surface sensitive. These measurements were performed at the Humboldt-Universität zu Berlin, using a JEOL JPS-9030 system with a base pressure of 2×10^{-9} mbar. A monochromatized aluminum K_α X-ray source (1486.6 eV) was used for excitation, yielding a setup resolution of about 0.6 eV. For the determination of atomic concentrations, sensitivity factors provided by JEOL, which were corrected for the angular asymmetry factors, were used (S_{O1s} = 17.60, $S_{Ga2p_{3/2}}$ = 94.42, S_{Al2p} = 2.82). A Shirley background was subtracted prior to peak area determination. The samples were measured after introduction to the system without further preparation. Transmission measurements to determine the optical bandgap were conducted in a PerkinElmer Lambda 19 spectrometer. To determine the thickness of the thin films on c-sapphire, a J. A. Woollam M2000 ellipsometer was used. The surface properties were determined employing a Park Systems XE-150 atomic force microscope (AFM) in the noncontact mode.

III. STABILIZATION OF κ-$(Al,Ga)_2O_3$

To determine the growth window regarding growth pressure, κ-$(Al,Ga)_2O_3$ thin films were grown on c-sapphire. The elliptically segmented target consists of $(Al_{0.1}Ga_{0.9})_2O_3$ with an additional admixture of 1 at. % SnO_2 in the outer segment. To exclude the influence of the tin amount in the particle flux of the PLD plasma, the radius of the PLD laser was kept constant such that a tin content of ≈0.8 at. % Sn in the PLD plasma was achieved for all samples. A total of 5000 pulses were applied for all thin films, resulting in film thicknesses of ≈110 nm for $p(O_2) = 3 \times 10^{-4}$ mbar and ≈200 nm for $p(O_2)$ = 0.01 mbar, respectively.

The crystal phase was determined from XRD 2θ-ω scans, as shown in Figs. 1(a) and 1(b). A distinction between the β-phase and κ-phase is observable comparing the peak positions and intensities of the 2θ-ω diffraction pattern. The κ-phase is (001) oriented and exhibits much higher intensities and narrower peaks compared to the β-phase that occurs for pressures of $p(O_2)$ = 0.02 mbar and higher. In the magnified view [Fig. 1(b)], the ($\bar{4}02$) peak of the β-phase is observed with low intensity prior to the (004) peak of the κ-phase independent of the growth pressure. This may be due to the formation of a thin β-$(Al,Ga)_2O_3$ layer between the substrate and the κ-$(Al,Ga)_2O_3$ thin film as it has been observed and verified by TEM measurements by Kracht *et al.* for ε-Ga_2O_3[20] grown by MBE. The incorporation of aluminum, as determined by EDX and indicated by the shift of the (004) and (006) peaks to higher angles (i.e., lower c-lattice constants) in the XRD 2θ-ω spectra, into the thin film is strongly pressure dependent. For $p(O_2)$ = 0.01 mbar, the transfer of aluminum from the target to the thin film is stoichiometric. For lower pressures, the transfer is nonstoichiometric with up to double the amount of aluminum incorporated into the thin film compared to the aluminum content of the target [Fig. 1(b)]. Therefore, in low pressure conditions, a favored Al-incorporation is present due to, *inter alia*, the energetically favored aluminum–oxygen bond with a bond dissociation energy of E_D(Al–O) = 5.30(4) eV compared to the lower dissociation energy of E_D(Ga–O) = 2.95(65) eV for the gallium oxide bond[38] and the desorption of volatile Ga_2O suboxides. If the oxygen pressure is increasing, more gallium gets incorporated into the thin film, and subsequently, the transfer becomes stoichiometric which is also reflected by an increased growth rate. For even higher oxygen pressures, it seems that the liquid tin layer on top of the thin film, which may act as a surfactant,[21] gets oxidized and crystallizes *in situ*. Therefore, the β-phase forms as the tin supply is not sufficient to maintain growth in the κ-phase.

To investigate the sole impact of aluminum in κ-$(Al,Ga)_2O_3$ thin films, the growth conditions were kept constant at $p(O_2)$ = 0.002 mbar and $T \approx 600$ °C and the variation of the aluminum content was achieved by variation of the vertical position (r_{PLD}) of the PLD laser spot on the rotating target. A schematic depiction of the target and the resulting laser track is shown in the inset of Fig. 1(c). For smallest radii ($r_{PLD} < 4$ mm), binary κ-Ga_2O_3 thin films will form. If r_{PLD} is large enough such that the PLD laser ablates the material from the outside segment of the ellipse, aluminum is introduced to the thin film and the aluminum content increases for increasing r_{PLD} as more material will be ablated from the target side with a high aluminum content. An analytical function to describe the evolution of the thin film composition under variation of r_{PLD} for stoichiometric transfer from target to thin film is given by us in Ref. 37. However, this model does not include nonidealities such as extended shape of the laser spot and the imperfect elliptical form of the inner segment. Therefore, simple Monte Carlo simulations were conducted to further improve the accuracy of the modeling of the expected thin film composition. As shown in Fig. 1(c), the model fits the dependence of the composition for this technique nicely with a stoichiometry transfer factor (i.e., the ratio between aluminum in the target and the grown thin film) of 1.7 at a growth pressure of $p(O_2)$ = 0.002 mbar and a growth temperature of $T \approx 600$ °C. The aluminum content was calculated from EDX, XPS, and the expected linear dependency of the *c*-lattice constant as a function of the aluminum content that has been determined by XRD measurements. For this, the composition-dependent *c*-lattice constants of layers with well-known aluminum content as measured by EDX and XPS were fitted, and from the fit parameters, the Al-contents of the other samples were determined. The exact dependency $c(x)$ will be derived below. To compare the growth of κ-Ga_2O_3 and the effects of aluminum to the well investigated β-$(Al,Ga)_2O_3$ alloy system, the growth rates and aluminum contents for β- and κ-phase layers were measured [Fig. 1(d)]. For β-Ga_2O_3, the growth is strongly affected by volatile Ga_2O

suboxides whose formation is heavily influenced by growth pressure and temperature leading to different film thickness and structural, morphological, and electrical properties.[39] If aluminum is introduced to the growth process in oxygen rich conditions, the amount of available oxygen is sufficient to fully oxidize both aluminum and gallium. Hence, the desorption of gallium suboxides is low such that stoichiometric transfer is observed [Fig. 1(d)]. If the oxygen offer is now reduced, the gallium and aluminum atoms start to compete over the available oxygen (metal rich conditions), and due to the energetically favored Al–O bond, aluminum is preferably incorporated and the gallium suboxides are desorbed more often, which results in lower growth rates for a fixed cation flux,[40] as depicted by red triangles in Fig. 1(d). For the case of an increasing Al/Ga ratio in the cation flux at constant pressure in the oxygen-poor regime [blue triangles in Fig. 1(d)], the varied cation ratio leads to a substitution of the gallium with aluminum in the growth process. Therefore, the amount of desorbed gallium suboxides decreases which would increase the growth rates if the aluminum content is increased without a change in the total particle flux, but due to ablation of the laser in the more aluminum rich area of the target, the absorption of the laser radiation is less efficient due to the low absorption of Al_2O_3 in this energy range such that the total amount of ablated material also decreases. This results in a lower total particle flux, which subsequently leads to a decrease in growth rates. In result, both effects, the increase in growth rate due to a reduction in gallium suboxides and the decrease in the growth rate due to lower ablation rates in the Al-rich segment, lead for the growth pressure of $p(O_2) = 0.002$ mbar to a nearly constant growth rate with increasing aluminum content as demonstrated by experiment in Fig. 1(d). In contrast, for the κ-phase, a decrease in growth rates is observed for higher aluminum contents; therefore, it is assumed that the formation or desorption of volatile Ga_2O suboxides is suppressed and the trend is solely determined by the lower ablation efficiency of the Al-rich target segment due to lower absorption of the PLD laser radiation. These findings support surfactant-mediated growth already proposed by Kneiß *et al.*[21] as the main mechanism of κ-Ga_2O_3 growth by tin-assisted PLD.

IV. LATTICE CONSTANTS

To verify the κ-phase growth and to investigate its crystallographic properties, XRD 2θ-ω and φ-scans were performed, as shown in Figs. 2(a), 2(c), and 2(d). Due to the incorporation of aluminum into the κ-Ga_2O_3 thin films, the (004) peaks visible in the presented 2θ-ω scans [Fig. 2(a)] shift to higher angles with increasing aluminum content which corresponds to decreasing c-lattice constants in the orthorhombic crystal structure. This is as expected due to the smaller ionic size of aluminum compared to gallium. If no additional template was used, the $(Al_xGa_{1-x})_2O_3$ thin films crystallize in the κ-phase up to $x \approx 0.38$ and no impurity or mixed phases were detectable. For even higher aluminum contents, only XRD amorphous thin films were obtained, indicating amorphous or microcrystalline growth. However, for growth on a κ-Ga_2O_3 template, the layers exhibit typical κ-phase reflections without the occurrence of side phases up to $x = 0.65$. For higher Al-contents, X-ray amorphous layers were obtained. Compared to

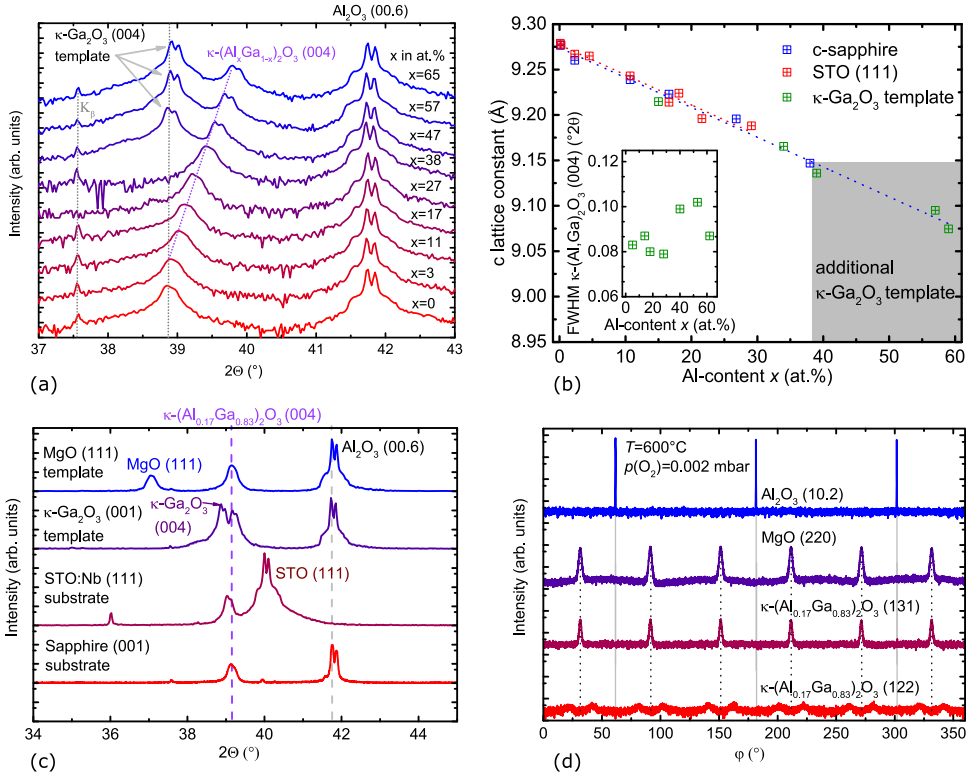

FIG. 2. (a) Typical XRD 2θ-ω scan of $(Al_xGa_{1-x})_2O_3$ thin films with variable x as indicated on c-sapphire ($x \leq 0.38$) and κ-Ga_2O_3 templates ($x > 0.38$). K_β denotes reflections due to K_β radiation. No mixed phase is visible. The κ-$(Al_xGa_{1-x})_2O_3$ (004) peak shifts clearly to higher angular positions with increasing aluminum content. (b) Evolution of the c-lattice constant as calculated from the κ-$(Al_xGa_{1-x})_2O_3$ (004), (006), (008), and (0010) peak positions. In the inset, the FWHM (full width at half maximum) of the κ-$(Al,Ga)_2O_3$ (004) peak for various Al-contents is shown for thin films with ≈250 nm thickness on a κ-Ga_2O_3 template. (c) Typical XRD 2θ-ω scans of κ-$(Al_xGa_{1-x})_2O_3$ grown on the indicated different substrates or templates, in the vicinity of the κ-Ga_2O_3 (004) peak. (d) Typical XRD φ-scans of MgO-buffered κ-$(Al_{0.17}Ga_{0.83})_2O_3$ thin films confirm epitaxial growth in three rotational domains.

κ-$(Al_xGa_{1-x})_2O_3$ thin films grown by MCVD on AlN templates produced on c-sapphire with a maximum aluminum content[36] of $x = 0.395$, these results display a significant increase in the maximum amount of incorporated aluminum. For β-$(Al_xGa_{1-x})_2O_3$ thin films, a maximum phase pure aluminum content of $x \approx 0.6$ was observed[41,42] until impurity phases occurred. Therefore, the maximum aluminum incorporation limit does not seem to depend on the respective Ga_2O_3 phase.

The XRD 2θ-ω full width at half maximums (FWHMs) of the κ-$(Al_xGa_{1-x})_2O_3$ (004) peak are depicted in the inset of Fig. 2(b). For thin films grown on a κ-Ga_2O_3 template, no distinct dependence on x is observable and the crystalline quality stays on a very high level for all aluminum contents and are on par to κ-Ga_2O_3 layers grown by PLD within our group.[21] The deposition on c-sapphire and STO(111):Nb substrates as well as on MgO(111) and κ-Ga_2O_3 templates resulted in thin films with three rotational domains as shown for MgO(111) templates as an example in Fig. 2(d). The corresponding in-plane lattice mismatch of κ-Ga_2O_3 compared to the employed substrate and template materials was calculated by Kneiß *et al.*[21]

The c-lattice constant was calculated utilizing the position of the XRD-(004), (006), (008) and (0010) κ-$(Al,Ga)_2O_3$ peaks to compensate the goniometer error. It is linearly decreasing with x in agreement with Vegard's law across the whole range of incorporated aluminum. For thin films grown on STO(111):Nb, no significant difference in the c-lattice constant is observable compared to thin films produced on c-sapphire hinting at relaxed growth. Similarly, the deposition on MgO and κ-Ga_2O_3 templates has no impact on the c-lattice constant compared to layers on c-sapphire [Fig. 2(c)]. The c-lattice constants for the layers on c-sapphire as well as on the κ-Ga_2O_3 templates were fitted linearly as shown in Fig. 2(b), delivering the following relationship:

$$c(x)(\text{Å}) = (9.274 \pm 0.004) - (0.328 \pm 0.010) \cdot x. \quad (1)$$

V. GROWTH ANALYSIS

To gain a deeper insight into the growth of the thin films, reciprocal space maps (RSM) of κ-$(Al_xGa_{1-x})_2O_3$ layers on c-sapphire and κ-Ga_2O_3 template in the vicinity of the (139) κ-Ga_2O_3 and (11.12) c-sapphire reflection were measured. Figures 3(a) and 3(b) show the RSMs of samples with the κ-Ga_2O_3 template. A dominant broadening in $q_\parallel$ is present and might be due to the small lateral domain size of the crystallites.[20] The peak positions of all investigated κ-$(Al_xGa_{1-x})_2O_3$ (139) thin film reflections are plotted in Fig. 3(d) in reciprocal space coordinates. If the trend evolved along the dashed line parallel to $q_\perp$ at the κ-Ga_2O_3 peak position, the thin films would have been pseudomorphically strained on the κ-Ga_2O_3 template. The evolution of these peak positions, however, follows the tilted line which represents the extrapolated linear connection between the origin of the coordinate system in reciprocal space and the position of the κ-Ga_2O_3 (139) peak. This behavior corresponds to fully relaxed growth for all investigated aluminum contents for the alloy layers grown on κ-Ga_2O_3 template as well as on c-sapphire. For aluminum contents $x \geq 0.38$, the broadening is tilted, which indicates increasing tilt mosaicity of the crystallites of the epilayer. Epitaxial growth is confirmed for all aluminum contents since the asymmetric peaks of the Al_2O_3 (11.12) substrate, κ-Ga_2O_3 (139) template, and κ-$(Al,Ga)_2O_3$ (139) are observable at the same φ-position the RSMs were measured. For corroboration whether the in-plane lattice constants follow Vegard's law, the in-plane distances d_{130} were determined for all samples by evaluating the $q_\parallel$-position of the κ-$(Al,Ga)_2O_3$ (139) reflection. The positions of the peaks were corrected to literature values of Al_2O_3 utilizing the JCPDS 82-1399 sheet. As shown in Fig. 3(c), the in-plane distances decrease almost linearly for the thin films on κ-Ga_2O_3 template. The corresponding relationship is given for layers grown on c-sapphire and the κ-Ga_2O_3 template, as displayed in Fig. 3(c). Unexpectedly, relaxed growth is observed even for the lowest investigated aluminum contents of $x = 0.10$. For these thin films, the in-plane lattice mismatch compared to the κ-Ga_2O_3 template is approximately 0.3%. This circumstance may be due to the large thickness of the thin film of approximately 150 nm–200 nm. Investigations of the strain relaxation of GaN/AlGaN heterostructures suggest a critical thickness of ≈100 nm for similar mismatches.[43,44] Therefore, pseudomorphic growth seems feasible for structures with smaller

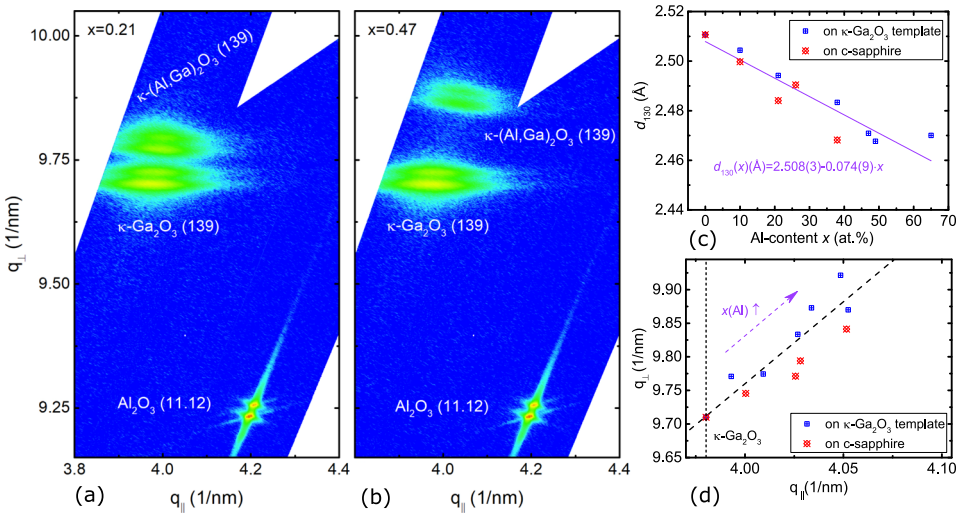

FIG. 3. Reciprocal space maps in the vicinity of the κ-Al_2O_3 (11.12) peak of κ-$(Al_xGa_{1-x})_2O_3$ thin films on κ-Ga_2O_3 template with $x = 0.21$ (a) and $x = 0.47$ (b). Epitaxial growth is observed for all compositions. All measured RSMs for thin films on c-sapphire and κ-Ga_2O_3 template can be found in the supplementary material. (c) Evolution of the in-plane d-spacing d_{130} for thin films on c-sapphire and κ-Ga_2O_3 template. The purple line represents the linear fit of the data for thin films grown on c-sapphire and κ-Ga_2O_3. (d) Positions of the κ-$(Al_xGa_{1-x})_2O_3$ (139) reflection peaks for thin films produced on κ-Ga_2O_3 template and on c-sapphire in reciprocal lattice units. The corresponding aluminum contents of the layers evolve as indicated by the purple arrow.

layer thicknesses, for example in quantum well heterostructures or superlattices.

VI. SURFACE PROPERTIES

The surface properties of κ-$(Al,Ga)_2O_3$ thin films on c-sapphire and STO(111):Nb substrates and MgO as well as κ-Ga_2O_3 templates were determined by AFM measurements, as depicted in Fig. 4. All samples were deposited under similar growth conditions, and the aluminum content was $x \approx 0.17$. For all investigated samples, the surfaces are very smooth; however, κ-$(Al_xGa_{1-x})_2O_3$ layers exhibit the smoothest surfaces on c-sapphire and STO(111):Nb substrates and MgO template. Even though the crystalline quality and the range of incorporated aluminum is the highest for κ-Ga_2O_3 buffered layers, the surface roughness of these thin films is the highest, which could also be due to the larger total thin film thickness. In terms of surface morphology, layers on MgO templates and STO(111):Nb substrates reveal small grains with sizes of ≈50 nm. For c-sapphire, the grain size increases slightly to ≈100 nm and reaches values of about 150 nm for layers on κ-Ga_2O_3 templates. The larger grain size of layers on the Ga_2O_3 buffer results in the higher surface roughness. If the aluminum content is increased while keeping the growth conditions constant, the surface roughness displays no coherent trend for layers on c-sapphire. As it was in case of the FWHM of the XRD κ-$(Al_xGa_{1-x})_2O_3$ (004) reflection, the roughness of κ-Ga_2O_3 buffered κ-$(Al_xGa_{1-x})_2O_3$ thin films exhibits no significant aluminum dependence and values of $R_q \approx (1.4 \pm 0.3)$ nm were measured, which are comparable to values of binary κ-Ga_2O_3 thin films[21] and more likely correlated with the grain size.

VII. OPTICAL PROPERTIES

To estimate the bandgap energies, transmission spectroscopy measurements were conducted on samples deposited on c-sapphire. For layers grown on κ-Ga_2O_3 template, only the absorption of the template layer would be detected and were therefore not investigated. Hence, the range of investigated aluminum contents is restricted by this measurement method to a maximum of $x = 0.38$. The obtained data of the direct bandgaps are presented in Fig. 5, and a linear increase is observed without obvious bandgap bowing for all investigated aluminum contents. A linear fit gives the following empirical relationship:

$$E_g(x)(\mathrm{eV}) = (4.91 \pm 0.03) + (2.27 \pm 0.02) \cdot x. \quad (2)$$

The range for bandgap engineering therefore is from 4.9 eV to 5.8 eV. These values are in good agreement with literature values for the aluminum κ-phase alloy[36] and are also surprisingly similar to literature data on the monoclinic alloy system.[5] However, for samples grown on the κ-Ga_2O_3 template, even higher bandgap values are expected if Eq. (2) is extrapolated to the highest aluminum content of $x = 0.65$, increasing the range of bandgap engineering to 6.4 eV. In combination with κ-$(In_xGa_{1-x})_2O_3$, this enables bandgap engineering with total band offsets corresponding to photon energies up to the green part of the visible spectrum with a total energy range of 2.2 eV (4.2 eV–6.4 eV).[34]

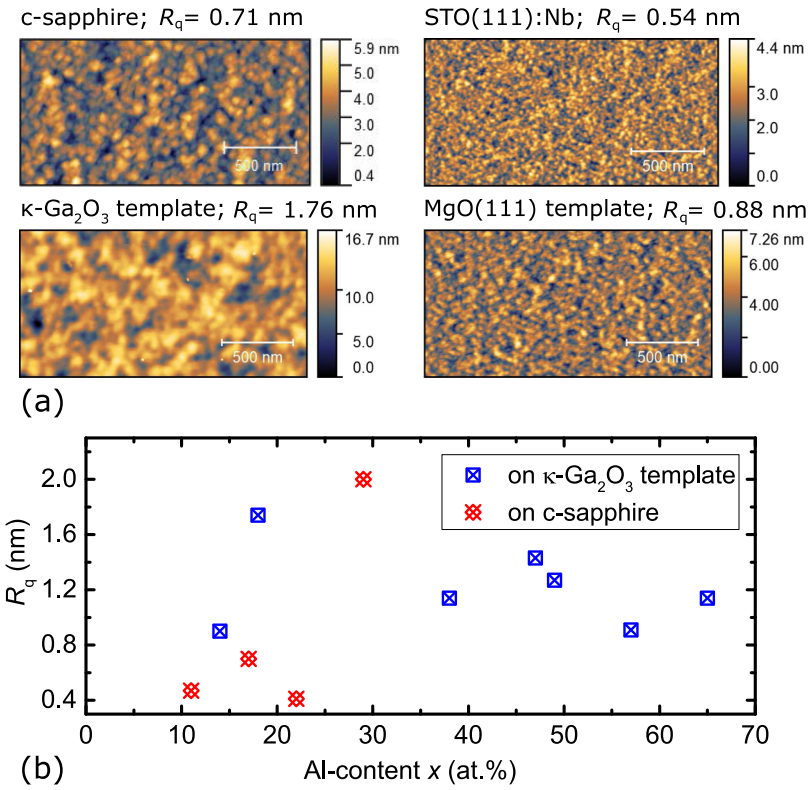

FIG. 4. (a) AFM surface morphology scans of an area of 2 μm × 1 μm of κ-$(Al_{0.17}Ga_{0.83})_2O_3$ thin films on various templates or substrates as indicated. (b) Root-mean squared surface roughness in dependence on the aluminum content. The surface morphology remains unchanged upon aluminum content variation and is therefore not depicted here.

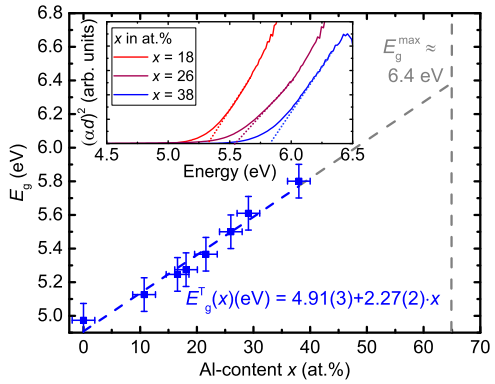

FIG. 5. Dependence of the bandgap estimated by transmission spectroscopy measurements on Al-contents up to $x = 0.38$. The dashed, gray line represents the extrapolation of the linear fit up to the highest aluminum content stabilized in κ-phase of $x = 0.65$. The $(\alpha d)^2$ absorbance spectrum is shown in the inset for three samples exemplary with linear extrapolations to zero absorption to estimate the bandgap energy.

VIII. CONCLUSION

In this report, the growth of phase-pure, high-quality κ-$(Al_xGa_{1-x})_2O_3$ thin films by PLD is demonstrated. By utilizing elliptically segmented targets (VCCS-PLD), we were able to fabricate all investigated samples with only two targets. For layers grown on c-sapphire, aluminum contents up to $x = 0.38$ were achieved. The application of an additional κ-Ga_2O_3 template increased the range significantly up to $x = 0.65$. Additionally, the growth on STO(111):Nb substrates and MgO(111) templates was investigated and showed comparable results to thin films on c-sapphire.

For all samples, epitaxial growth on all investigated substrate materials and template layers was verified. RSM measurements of κ-$(Al_xGa_{1-x})_2O_3$ layers on c-sapphire as well as κ-Ga_2O_3(001) template layers confirm relaxed growth for all aluminum contents. The in- and out-of-plane lattice constants obey Vegard's law.

Investigations of growth rates in regimes with constant growth conditions or constant aluminum amount at the target suggest that the formation or desorption of Ga_2O suboxides is suppressed for the growth of κ-Ga_2O_3. Surfactant-mediated epitaxy as likely growth mechanism was already proposed by our group and is in line with the current experimental results.[21]

The surface morphology was investigated, and smooth surfaces ($R_q \approx 1.4$ nm) independent of the aluminum content were verified. Therefore, it is concluded that the aluminum incorporation has no noteworthy impact on structural and morphological properties of nanocrystalline κ-$(Al_xGa_{1-x})_2O_3$ thin films. These results show that κ-$(Al,Ga)_2O_3$ is suitable for the growth of high-quality heterostructures in the κ-$(Al,Ga)_2O_3$ alloy system as long as the properties remain unchanged upon growth in non-nanocrystalline regimes. Therefore, it might be a promising choice as a barrier layer in heterostructure devices acting complementary to the κ-$(In_xGa_{1-x})_2O_3$ alloy as active quantum-well material. Exploiting the predicted high spontaneous polarization the formation of 2DEGs by polarization doping may be feasible at κ-Ga_2O_3/κ-$(Al_xGa_{1-x})_2O_3$ heterointerfaces.

The optical bandgap values are in good agreement with literature values.[36] The measurements performed for thin films up to $x = 0.38$ and bandgaps up to 5.8 eV were measured with expected values up to 6.4 eV. In combination with κ-$(In_xGa_{1-x})_2O_3$ layers, values from 4.2 eV[34] to 6.4 eV are expected, extending the range of band offsets in heterostructures into the green part of the visible spectrum.

These results support the promising prospects of κ-Ga_2O_3 and its alloys in solar-blind infrared detectors or high electron mobility transistors. However, for that, the growth of conductive κ-Ga_2O_3 by PLD, the suppression of rotational domains, and the high-quality growth of more sophisticated heterostructures such as superlattices should be tackled.

SUPPLEMENTARY MATERIAL

See the supplementary material for additional reciprocal space map measurements and XRD 2θ-ω scans.

ACKNOWLEDGMENTS

We are indebted to Monika Hahn for the fabrication of the PLD targets and Holger Hochmuth for the implementation of the VCCS-PLD in the growth setup. We also thank Ulrike Teschner for the transmission measurements and Jörg Lenzner for the EDX measurements. This work was supported by the European Social Fund within the Young Investigator Group "Oxide Heterostructures" (Grant No. SAB 100310460). M.K. and A.H. also acknowledge the Leipzig School of Natural Sciences BuildMoNa. The work in Berlin was funded by the Deutsche Forschungsgemeinschaft (DFG)—Project No. 182087777-SFB 951.

REFERENCES

[1] T. Matsumoto, M. Aoki, A. Konoshita, and T. Aono, "Absorption and reflection of vapor grown single crystal platelets of β-Ga_2O_3," Jpn. J. Appl. Phys., Part 1 **13**, 1578 (1974).

[2] M. Higashiwaki, K. Sasaki, A. Kuramata, T. Masui, and S. Yamakoshi, "Gallium oxide (Ga_2O_3) metal-semiconductor field-effect transistors on single-crystal β-Ga_2O_3 (010) substrates," Appl. Phys. Lett. **100**, 013504 (2012).

[3] S. J. Pearton, J. Yang, P. H. Cary, J. Kim, M. J. Tadjer, and M. A. Mastro, "A review of Ga_2O_3 materials, processing, and devices," Appl. Phys. Rev. **5**, 011301 (2018).

[4] S. I. Stepanov, V. I. Nikolaev, V. E. Bougrov, and A. E. Romanov, "Gallium oxide: Properties and applications—A review," Rev. Adv. Mater. Sci. **44**, 63–86 (2016).

[5] H. von Wenckstern, "Group-III sesquioxides: Growth, physical properties and devices," Adv. Electron. Mater. **3**, 1600350 (2017).

[6] I. Cora, F. Mezzadri, F. Boschi, M. Bosi, M. Čaplovičová, G. Calestani, I. Dódony, B. Pécz, and R. Fornari, "The real structure of ε-Ga_2O_3 and its relation to κ-phase," CrystEngComm **19**, 1509–1516 (2017).

[7] J. Kim, D. Tahara, Y. Miura, and B. G. Kim, "First-principle calculations of electronic structures and polar properties of (κ,ε)-Ga_2O_3," Appl. Phys. Express **11**, 061101 (2018).

[8] M. B. Maccioni and V. Fiorentini, "Phase diagram and polarization of stable phases of $(Ga_xIn_{1-x})_2O_3$," Appl. Phys. Express **9**, 041102 (2016).

[9] S. B. Cho and R. Mishra, "Epitaxial engineering of polar ε-Ga_2O_3 for tunable two-dimensional electron gas at the heterointerface," Appl. Phys. Lett. **112**, 162101 (2018).

[10] Y. Zhuo, Z. Chen, W. Tu, X. Ma, Y. Pei, and G. Wang, "β-Ga_2O_3 versus ε-Ga_2O_3: Control of the crystal phase composition of gallium oxide thin film prepared by metal-organic chemical vapor deposition," Appl. Surf. Sci. **420**, 802–807 (2017).

[11] M. Mulazzi, F. Reichmann, A. Becker, W. M. Klesse, P. Alippi, V. Fiorentini, A. Parisini, M. Bosi, and R. Fornari, "The electronic structure of ε-Ga_2O_3," APL Mater. **7**, 022522 (2019).
[12] X. Xia, Y. Chen, Q. Feng, H. Liang, P. Tao, M. Xu, and D. Guotong, "Hexagonal phase-pure wide band gap ε-Ga_2O_3 films grown on 6H-SiC substrates by metal organic chemical vapor deposition," Appl. Phys. Lett. **108**, 202103 (2016).
[13] R. Fornari, M. Pavesi, V. Montedoro, D. Klimm, F. Mezzadri, I. Cora, B. Pécz, F. Boschi, A. Parisini, A. Baraldi, C. Ferrari, E. Gombia, and M. Bosi, "Thermal stability of ε-Ga_2O_3 polymorph," Acta Mater. **140**, 411–416 (2017).
[14] F. Mezzadri, G. Calestani, F. Boschi, D. Delmonte, M. Bosi, and R. Fornari, "Crystal structure and ferroelectric properties of ε-Ga_2O_3 films grown on (0001)-sapphire," Inorg. Chem. **55**, 12079–12084 (2016).
[15] Y. Chen, X. Xia, H. Liang, Q. Abbas, Y. Liu, and G. Du, "Growth pressure controlled nucleation epitaxy of pure phase ε- and β-Ga_2O_3 films on Al_2O_3 via metal-organic chemical vapor deposition," Cryst. Growth Des. **18**, 1147–1154 (2018).
[16] Y. Oshima, E. G. Víllora, Y. Matsushita, S. Yamamoto, and K. Shimamura, "Epitaxial growth of phase-pure ε-Ga_2O_3 by halide vapor phase epitaxy," J. Appl. Phys. **118**, 085301 (2015).
[17] H. Nishinaka, D. Tahara, and M. Yoshimoto, "Heteroepitaxial growth of ε-Ga_2O_3 thin films on cubic (111) MgO and (111) yttria-stablized zirconia substrates by mist chemical vapor deposition," Jpn. J. Appl. Phys., Part 2 **55**, 1202BC (2016).
[18] D. Tahara, H. Nishinaka, S. Morimoto, and M. Yoshimoto, "Heteroepitaxial growth of ε-Ga_2O_3 thin films on cubic (111) GGG substrates by mist chemical vapor deposition," in *2017 IEEE International Meeting for Future of Electron Devices, Kansai (IMFEDK)* (IEEE, 2017), Vol. 47.
[19] X. Zhao, Y. Zhi, W. Cui, D. Guo, Z. Wu, P. Li, L. Li, and W. Tang, "Characterization of hexagonal ε-$Ga_{1.8}Sn_{0.2}O_3$ thin films for solar-blind ultraviolet applications," Opt. Mater. **62**, 651–654 (2016).
[20] M. Kracht, A. Karg, J. Schörmann, M. Weinhold, D. Zink, F. Michel, M. Rohnke, M. Schowalter, B. Gerken, A. Rosenauer, P. J. Klar, J. Janek, and M. Eickhoff, "Tin-assisted synthesis of ε-Ga_2O_3 by molecular beam epitaxy," Phys. Rev. Appl. **8**, 054002 (2017).
[21] M. Kneiß, A. Hassa, D. Splith, C. Sturm, H. von Wenckstern, T. Schultz, N. Koch, M. Lorenz, and M. Grundmann, "Tin-assisted heteroepitaxial PLD-growth of κ-Ga_2O_3 thin films with high crystalline quality," APL Mater. **7**, 022516 (2019).
[22] M. Orita, H. Hiramatsu, H. Ohta, M. Hirano, and H. Hosono, "Preparation of highly conductive, deep-ultraviolet transparent β-Ga_2O_3 thin films at low temperature," Thin Solid Films **411**, 134 (2002).
[23] A. Parisini, A. Bosio, V. Montedoro, A. Gorreri, A. Lamperti, M. Bosi, G. Garulli, S. Vantaggio, and R. Fornari, "Si and Sn doping of ε-Ga_2O_3 layers," APL Mater. **7**, 031114 (2019).
[24] C. Kranert, M. Jenderka, J. Lenzner, M. Lorenz, H. von Wenckstern, R. Schmidt-Grund, and M. Grundmann, "Lattice parameters and Raman-active phonon modes of β-$(Al_xGa_{1-x})_2O_3$," J. Appl. Phys. **117**, 125703 (2015).
[25] S. Krishnamoorthy, Z. Xia, C. Joishi, Y. Zhang, J. Mcglone, J. Johnson, A. R. Arehart, J. Hwang, S. Lodha, S. Rajan, S. Krishnamoorthy, Z. Xia, C. Joishi, Y. Zhang, S. Lodha, and S. Rajan, "Modulation-doped β-$(Al_{0.2}Ga_{0.8})_2O_3/Ga_2O_3$ field-effect transistor," Appl. Phys. Lett. **111**, 023502 (2017).
[26] Y. Zhang, A. Neal, Z. Xia, C. Joishi, Y. Zheng, S. Bajaj, M. Brenner, S. Mou, D. Dorsey, K. Chabak, G. Jessen, J. Hwang, J. Heremans, and S. Rajan, "High mobility two-dimensional electron gas in modulation-doped β-$(Al_xGa_{1-x})_2O_3/Ga_2O_3$ heterostructures," e-print arXiv:1802.04426 (2018).
[27] C. Kranert, J. Lenzner, M. Jenderka, M. Lorenz, H. von Wenckstern, R. Schmidt-Grund, and M. Grundmann, "Lattice parameters and Raman-active phonon modes of $(In_xGa_{1-x})_2O_3$ for $x \leq 0.4$," J. Appl. Phys. **116**, 013505 (2014).
[28] T. Oshima and S. Fujita, "Properties of Ga_2O_3-based $(In_xGa_{1-x})_2O_3$ alloy thin films grown by molecular beam epitaxy," Phys. Status Solidi C **5**, 3113–3115 (2008).
[29] X. Liu and C.-K. Tan, "Electronic properties of monoclinic $(In_xGa_{1-x})_2O_3$ alloys by first-principle," AIP Adv. **9**, 035318 (2019).
[30] H. von Wenckstern, D. Splith, M. Purfürst, Z. Zhang, C. Kranert, S. Müller, M. Lorenz, and M. Grundmann, "Structural and optical properties of $(In,Ga)_2O_3$ thin films and characteristics of Schottky contacts thereon," Semicond. Sci. Technol. **30**, 024005 (2015).
[31] F. Zhang, K. Saito, T. Tanaka, M. Nishio, M. Arita, and Q. Guo, "Wide bandgap engineering of $(Al,Ga)_2O_3$ films," Appl. Phys. Lett. **105**, 162107 (2014).
[32] H. von Wenckstern, "Properties of $(In,Ga)_2O_3$ alloys," in *Gallium Oxide* (Elsevier, 2019), pp. 119–148.
[33] Y. Oshima, E. Ahmadi, S. C. Badescu, F. Wu, and J. S. Speck, "Composition determination of β-$(Al_xGa_{1-x})_2O_3$ layers coherently grown on (010) β-Ga_2O_3 substrates by high-resolution X-ray diffraction," Appl. Phys. Express **9**, 061102 (2016).
[34] A. Hassa, H. Von Wenckstern, D. Splith, C. Sturm, M. Kneiß, V. Prozheeva, and M. Grundmann, "Structural, optical, and electrical properties of orthorhombic κ-$(In_xGa_{1-x})_2O_3$ thin films," APL Mater. **7**, 022525 (2019).
[35] H. Nishinaka, N. Miyauchi, D. Tahara, S. Morimoto, and M. Yoshimoto, "Incorporation of indium into ε-gallium oxide epitaxial thin films grown: Via mist chemical vapour deposition for bandgap engineering," CrystEngComm **20**, 1882–1888 (2018).
[36] D. Tahara, H. Nishinaka, S. Morimoto, and M. Yoshimoto, "Heteroepitaxial growth of ε-$(Al_xGa_{1-x})_2O_3$ alloy films on *c*-plane AlN templates by mist chemical vapor deposition," Appl. Phys. Lett. **112**, 152102 (2018).
[37] M. Kneiß, P. Storm, G. Benndorf, M. Grundmann, and H. Von Wenckstern, "Combinatorial material science and strain engineering enabled by pulsed laser deposition using radially segmented targets," ACS Comb. Sci. **20**, 643–652 (2018).
[38] R. T. Sanderson, *Chemical Bonds and Bond Energy* (Academic Press, 1976).
[39] S. Müller, H. von Wenckstern, D. Splith, F. Schmidt, and M. Grundmann, "Control of the conductivity of Si-doped β-Ga_2O_3 thin films via growth temperature and pressure," Phys. Status Solidi A **211**, 34–39 (2014).
[40] A. Hassa, H. von Wenckstern, L. Vines, and M. Grundmann, "Influence of oxygen pressure on growth of Si-doped β-$(Al_xGa_{1-x})_2O_3$ thin films on c-sapphire substrates by pulsed laser deposition," ECS J. Solid State Sci. Technol. **8**, Q3217–Q3220 (2019).
[41] T. Oshima, T. Okuno, N. Arai, Y. Kobayashi, and S. Fujita, "β-$Al_{2x}Ga_{2-2x}O_3$ thin film growth by molecular beam epitaxy," Jpn. J. Appl. Phys., Part 1 **48**, 070202 (2009).
[42] A. L. Jaromin and D. D. Edwards, "Subsolidus phase relationships in the Ga_2O_3-Al_2O_3-TiO_2 system," J. Am. Ceram. Soc. **88**, 2573–2577 (2005).
[43] S. J. Hearne, J. Han, S. R. Lee, J. A. Floro, D. M. Follstaedt, E. Chason, and I. S. T. Tsong, "Brittle-ductile relaxation kinetics of strained AlGaN/GaN heterostructures," Appl. Phys. Lett. **76**, 1534–1536 (2000).
[44] S. R. Lee, D. D. Koleske, K. C. Cross, J. A. Floro, K. E. Waldrip, A. T. Wise, and S. Mahajan, "*In situ* measurements of the critical thickness for strain relaxation in AlGaN/GaN heterostructures," Appl. Phys. Lett. **85**, 6164–6166 (2004).